



**HAL**  
open science

# The Wide Swath Significant Wave Height: An Innovative Reconstruction of Significant Wave Heights from CFOSAT's SWIM and Scatterometer Using Deep Learning

J. K. Wang, Lofti Aouf, Alice Dalphinet, Y. G. Zhang, Y. Xu, Danièle Hauser,  
J. Q. Liu

## ► To cite this version:

J. K. Wang, Lofti Aouf, Alice Dalphinet, Y. G. Zhang, Y. Xu, et al.. The Wide Swath Significant Wave Height: An Innovative Reconstruction of Significant Wave Heights from CFOSAT's SWIM and Scatterometer Using Deep Learning. *Geophysical Research Letters*, 2021, 48 (6), pp.e2020GL091276. 10.1029/2020GL091276 . insu-03008979v1

**HAL Id: insu-03008979**

**<https://insu.hal.science/insu-03008979v1>**

Submitted on 17 Nov 2020 (v1), last revised 19 Mar 2021 (v2)

**HAL** is a multi-disciplinary open access archive for the deposit and dissemination of scientific research documents, whether they are published or not. The documents may come from teaching and research institutions in France or abroad, or from public or private research centers.

L'archive ouverte pluridisciplinaire **HAL**, est destinée au dépôt et à la diffusion de documents scientifiques de niveau recherche, publiés ou non, émanant des établissements d'enseignement et de recherche français ou étrangers, des laboratoires publics ou privés.

1     **The Wide Swath Significant Wave Height: An Innovative Reconstruction of Significant**  
2     **Wave Heights from CFOSAT’s SWIM and Scatterometer Using Deep Learning**

3  
4     **J. K. Wang<sup>1\*</sup>, L. Aouf<sup>2\*</sup>, A. Dalphin<sup>2</sup>, Y. G. Zhang<sup>3</sup>, Y. Xu<sup>3</sup>, D. Hauser<sup>4</sup> and J. Q. Liu<sup>3</sup>**

5     <sup>1</sup> National Marine Environmental Forecasting Center, 100081, Beijing, China.

6     <sup>2</sup> Météo-France, 31057, Toulouse, France.

7     <sup>3</sup> National Satellite Ocean Application Service, 100081, Beijing, China.

8     <sup>4</sup> LATMOS/IPSL, 78280, Guyancourt, France

9  
10    Corresponding author: J. K. Wang (wangjiuke@nmefc.cn); L. Aouf (lotfi.aouf@meteo.fr)

11  
12    **Key Points:**

- 13     • An innovative method for extending significant wave height (SWH) from nadir to a wide  
14     swath is presented.
- 15     • A deep neural network (DNN) model is developed based on simultaneous observations  
16     from the nadir beam and wind scatterometer of the CFOSAT.
- 17     • Significant positive impacts are found in the assimilation of the ‘wide swath’ SWH  
18     compared to the assimilation of the SWIM nadir only.

**21 Abstract**

22 The accuracy of a wave model can be improved by assimilating an adequate number of  
23 remotely sensed wave heights. The Surface Waves Investigation and Monitoring (SWIM) and  
24 Scatterometer (SCAT) instruments onboard China-France Oceanic SATellite (CFOSAT) provide  
25 simultaneous observations of waves and wide swath wind fields. Based on these synchronous  
26 observations, a method for retrieving the SWH over an extended swath is developed using the  
27 deep neural network (DNN) approach. With the combination of observations from both SWIM  
28 and SCAT, the SWH estimates achieve significantly increased spatial coverage and promising  
29 accuracy. As evidenced by the assessments of assimilation experiments, the assimilation of this  
30 ‘wide swath SWH’ achieves an equivalent or better accuracy than the assimilation of the  
31 traditional nadir SWH alone and enhances the positive impact when assimilated with the nadir  
32 SWH. Therefore, insights into the better utilization of wave remote sensing in assimilation are  
33 presented.

**34 Plain Language Summary**

35 Data assimilation is an effective way to improve wave numerical simulations, and its impact  
36 is related to both the quality and the quantity of wave observations. China-France Oceanic  
37 SATellite (CFOSAT) carries two instruments, namely, Surface Waves Investigation and  
38 Monitoring (SWIM) and a scatterometer (SCAT), which are designed to provide along-track  
39 wave parameters and wind observations over a wide swath, respectively. By combining  
40 observations from both instruments, we propose a method to estimate the SWH (significant wave  
41 height) over a wide swath (typically  $\pm 100$  km on each side of the nadir track) that aims to  
42 achieve an accuracy as good as the SWIM nadir and an improved spatial coverage. The method  
43 is developed by using the deep neural network (DNN) approach. With the advantage of both a  
44 significantly increased spatial coverage and reasonable accuracy, the wide swath SWH has the  
45 potential to enhance the positive impacts of wave assimilation. Assimilation experiments  
46 demonstrate that the wide swath SWH achieves impacts as good as the assimilation of the SWIM  
47 nadir SWH and enhances the accuracy of the wave model when assimilated together with the  
48 nadir SWH. Hence, synchronous observations from CFOSAT will facilitate relevant applications  
49 in operational wave forecasting.

## 50 **1 Introduction**

51 A better description of the sea state directly leads to better wave climate evaluations and  
52 climate projections of sea level in coastal areas. The significant wave height (SWH) is the most  
53 widely used indicator to measure the sea state. Therefore, it is critical to accurately monitor and  
54 forecast the SWH, and extensive studies have been performed to improve the accuracy of wave  
55 observations in this context. Data assimilation has been shown to be an effective method to  
56 improve numerical forecasts by reducing the error of the initial field from observations (Daley  
57 1993). The assimilation of wave observations is proved to be able to have an obvious positive  
58 impact on the model accuracy (Lionello et al., 1992). From another perspective, due to the  
59 principles of a numerical wave model, an adequate number of wave observations must be  
60 assimilated into the model to implement continuous corrections against the deviation introduced  
61 by the forcing (Portilla, 2009). Therefore, increasing both the quality and the quantity of wave  
62 observations is critical for improving the wave forecast accuracy, which is exactly the objective  
63 of developing new wave observation methods.

64 Wave buoys are the most traditional method of measuring waves, as they can provide the  
65 most comprehensive information (Hasselmann et al., 1980; Steele et al. 1992) and thus be used  
66 as a reference. However, the distribution of wave buoys is severely limited due to costs. The  
67 rapid development of wave remote sensing, a promising alternative, has been extremely  
68 meaningful to wave forecasting and related studies. The spaceborne radar altimeter has become  
69 the major instrument for the acquisition of SWH observations (Fedor et al., 1979; Hayne, 1980;  
70 Dobson et al., 1987). Through decades of improvement in the related hardware and processing  
71 algorithms (Cotton et al., 1994; Liu et al., 2016), modern operational altimeters, such as the  
72 Jason series (Nerem et al., 2010) and HY2 series (Jiang et al., 2012), provide global SWH  
73 observations along their nadir tracks with high accuracy. The significant increase in the quantity  
74 of wave observations from altimeters has surely led to valuable improvements in the impacts of  
75 data assimilation (Lionello et al., 1992; Breivik et al., 1994; Bhatt et al., 2005; Emmanouil et al.,  
76 2007; Cao et al., 2015, Aouf et al. 2015). However, altimeter observations are still limited to  
77 their nadir tracks, limiting the number of observations.

78 The SWIM (Surface Waves Investigation and Monitoring) instrument carried by CFOSAT  
79 (China-France Oceanic SATellite) was launched in 2018. SWIM is a new and unique instrument

80 that can provide two additional sets of observations of wave spectra observations at wavelengths  
81 from 70m to 500m from each side of the altimeter nadir (Hauser et al., 2016; Xu et al. 2019).  
82 Moreover, CFOSAT also carries a microwave scatterometer (SCAT) that works simultaneously  
83 with SWIM to obtain a wind field with high accuracy across a wide swath of approximately 800  
84 km (Lin et al., 2018). Wind is the source of wave energy, so the possibility exists for SWH  
85 observations to be extended from the nadir to a swath covered by SCAT, the so-called ‘wide  
86 swath SWH’. The wide swath SWH, which has scarcely been investigated and discussed  
87 heretofore, is obtained by extracting synchronously observed information from both SWIM and  
88 SCAT. Therefore, together with the SWIM nadir, the addition of the wide swath SWH could  
89 significantly increase the quantities of wave observations comparing to that of originally  
90 designed SWIM products, which would potentially further improve wave forecasts with data  
91 assimilation.

92 In this paper, we present a novel method for obtaining the SWH over a wide swath from the  
93 synchronous observations of SWIM and SCAT. A retrieval model based on a deep neural  
94 network (DNN) is established and trained using the SWH acquired from state-of-the-art high-  
95 accuracy altimeters, namely, Jason-3 and SARAL (Abdalla, 2015; Yang et al., 2020). The  
96 method and dataset used in the DNN to estimate the SWH over SCAT grid points at a swath  
97 distance of up to 200 km are described in section 2. The SWH estimated over this wide swath is  
98 validated in section 3. In section 4, the results of assimilation experiments are described to  
99 provide a comprehensive and fundamental confirmation of the impact of the newly estimated  
100 wide swath SWH. The validation of the assimilation of the wide swath SWH reveals an  
101 improvement in the model accuracy compared with the assimilation of the nadir SWH only,  
102 which offers evidence for the benefit of the wide swath wave product.

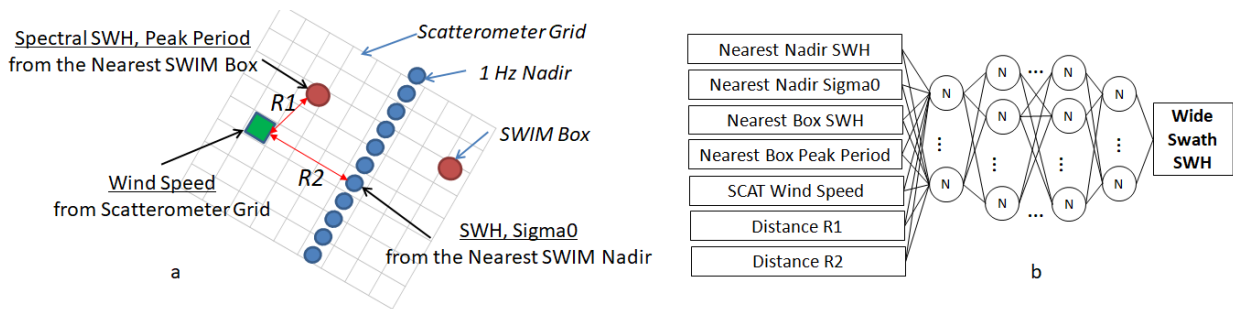
103

## 104 **2 Data Setup and Method**

105 The setup of the observations from CFOSAT is indicated in Figure 1a. The unique  
106 synchronous observations from the SCAT and SWIM instruments used to obtain simultaneous  
107 wind and wave information are described here. First, SWIM can provide the nadir total SWH  
108 similar to traditional altimeters. In addition, SWIM observes two additional ‘boxes’ containing  
109 wave directional spectra distributed on either side of the nadir track. However, only the waves

110 whose wavelengths range from 70 m to 500 m can be observed in these boxes (Hauser et al.,  
 111 2020). The distance between the boxes and the nadir track is approximately 50km. Second, a  
 112 wide swath of the wind field, including both wind speed and wind direction data, can be obtained  
 113 from SCAT.

114 The wind observations cover a larger region than the SWIM nadir and boxes. The key idea  
 115 of retrieving the wide swath SWH is to acquire the total SWH by extracting the information from  
 116 both wind and wave observations, in other words, to obtain more SWH observations by  
 117 converting some ‘wind grids’ from SCAT into ‘SWH grids’ from the combination with SWIM  
 118 observations. Being a widely used method in the field of deep learning, the deep neural network  
 119 (DNN) is a powerful technique for refining features and information from big data. The  
 120 efficiency and robustness of DNN have been demonstrated in classification, data mining and  
 121 other fields, and DNN has been shown to be effective when applied to wave remote sensing  
 122 (Wang et al., 2020). Thus, we build the wide swath SWH retrieval model based on DNN.



123  
 124 **Figure 1.** Schematic diagram of retrieving the wide swath SWH. Panel 1a shows a schematic of  
 125 the observations made with SWIM and SCAT onboard CFOSAT. The boxes and nadir samples  
 126 from SWIM are marked as red and blue circles, respectively. The wind speed grids are shown in  
 127 gray, and the green square is one of these SCAT grids. The distances from this grid to the nearest  
 128 SWIM box and nadir point are defined as R1 and R2, respectively. Panel 2b indicates the  
 129 structure of the DNN model for the retrieval of the wide swath SWH.

130 The structure of the DNN model is presented in Figure 1b. Seven parameters are used as the  
 131 inputs. Wind speed data from the SCAT grid can be seen as information highly related to the  
 132 windsea. The SWH and peak period from the SWIM boxes can provide the wave information  
 133 (over wavelengths from 70 m to 500 m) for the DNN model, approximately compensating for the  
 134 missing wave energy if the wave information is obtained only from the SCAT wind speed grid.

135 The nadir total SWH from SWIM is used as an important reference for the estimation of the wide  
136 swath SWH. The sigma0 (backscattered cross section) from the nadir track is also an important  
137 parameter that is highly related to the sea surface roughness, giving the model the information  
138 regarding the sea state as it is related to both the wind speed and the SWH. R1 and R2 are also  
139 included in the DNN model as indicators of the impacts from the SWIM boxes and nadir.

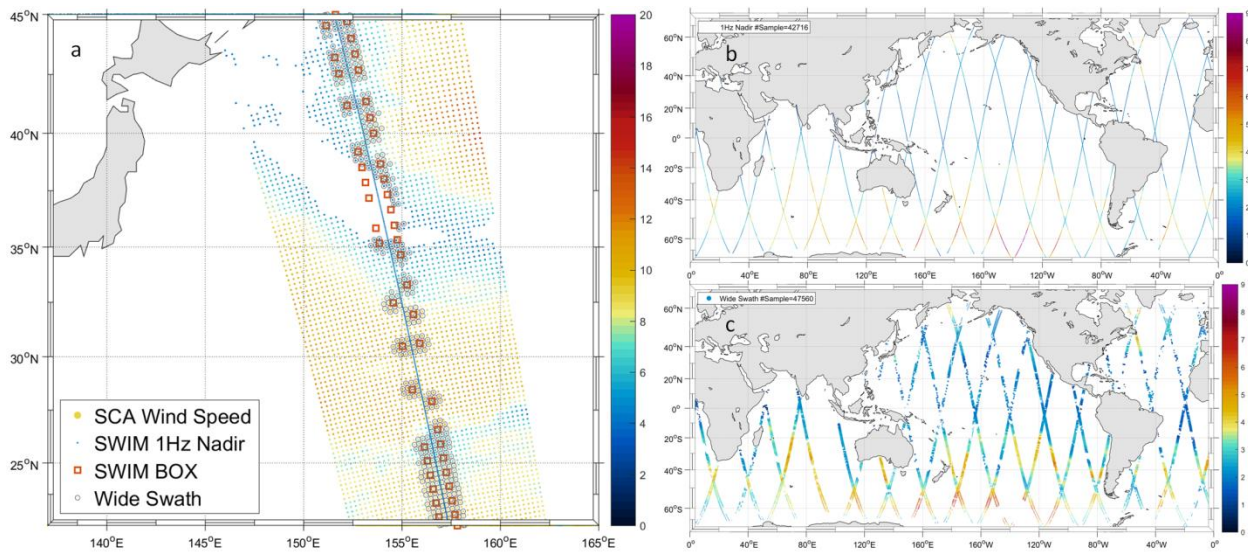
140 The model comprises 6 layers of neurons. The rectified linear unit (ReLU, Nair et al., 2010)  
141 is used as the activation function in each neuron of the DNN model. The parameters of DNN,  
142 such as the weights between the neurons of layers, are determined by ‘supervised training’, that  
143 is, an iterative algorithm that updates these parameters depending on the calculation of the ‘loss’  
144 between the DNN output and the truth. The SWH data from the collocated observations of the  
145 Jason-3 and SARAL altimeters are used as the truth to train the wide swath DNN model. The  
146 distance between the SCAT grid and altimeter is limited to less than 12.5 km, and the time  
147 window is  $\pm 30$  min. The periods of the collocated data range from April to June 2019 and from  
148 January to February 2020. There are 6090 match-ups between CFOSAT and Jason-3/SARAL; 75%  
149 of these match-ups are used to train the DNN model, while the other 25% are used as the  
150 independent dataset for validation.

151

### 152 **3 Wide Swath SWH Estimation and Accuracy**

153 An example of the geographical coverage of actual CFOSAT observations is presented in  
154 Figure 2 to show the distributions of nadir and non-nadir data. The SWH estimates from the  
155 SWIM nadir beam are oriented along the nadir track (blue line in Figure 2), and spectral wave  
156 information is given up to approximately 50 km on either side of the nadir track (red squares in  
157 Figure 2), while wind speeds and directions are provided from SCAT measurements along a  
158 swath of approximately 800 km. As shown in Figure 2, some SWIM and SCAT data points are  
159 missing because they have been rejected during quality control. As is typical for the spatial  
160 criterion of collocation during the assessment of altimeter measurements, we assume that the  
161 SWH observations inside a 50 km radius are highly related. Therefore, considering the relevant  
162 radius of wave impact, we limit R1 to 50 km, which makes R2 equal to 100 km. Under this  
163 setting, the SCAT wind grids within a distance of 100 km from nadir are transitioned into wave  
164 grids for the DNN model. Therefore, we now obtain a 200 km swath of wave observations at a

165 resolution of 25 km (the spatial resolution of SCAT), which are marked as gray circles in Figure  
 166 2. It can be clearly noted that the spatial coverage of wave observations is significantly increased  
 167 compared to the original SWIM observations. The distributions of nadir and wide swath SWH  
 168 observations acquired over a 24-hour period are presented in Figure 2b and 2c, respectively.  
 169 There are 42176 samples from the SWIM nadir and 47560 samples from the wide swath SWH. It  
 170 should be noted that the wide swath SWH can not only provide the same amount of data as the  
 171 SWIM nadir but also cover a larger area of the ocean surface.



172

173 **Figure 2.** Geometry used for the wide swath SWH retrieval. Panel 2a shows the locations of the  
 174 CFOSAT observations at 07 UTC on 1 May 2019. SWIM wave boxes and nadir data are marked  
 175 as red boxes and blue points, respectively. The wind grid points from CFOSAT SCAT are  
 176 marked as colored points, and the wide swath SWH grid points are indicated as gray circles. The  
 177 distributions of the nadir and wide swath SWH observations acquired over a 24-hour period are  
 178 presented in 2b and 2c, respectively.

179 In addition to the significant improvements in the amount of data and spatial coverage, the  
 180 accuracy of the wide swath SWH is also validated against the independent match-ups with Jason-  
 181 3 and SARAL. Five statistical parameters, namely, the bias, mean absolute error (MAE), root  
 182 mean square error (RMSE), normalized root mean square error (NRMSE) and scatter index (SI),  
 183 are used in the validation (Yang et al., 2020). A good scatter pattern of 1580 samples is achieved  
 184 with bias of only 0.001m, obtaining small MAE, RMSE, NRMSE and SI values of 0.181m,  
 185 0.257 m 8.2% and 8.2%, respectively. An unbiased SWH and a reasonable RMSE can be

186 achieved over most of the SWH range, and satisfactory NRMSE and SI values (both under 10%)  
187 can be found when the SWH is above 1m. The validation of the wide swath SWH demonstrates  
188 an accuracy equivalent to that of the SWIM nadir SWH or state-of-the-art altimeters.

189 Consequently, the wide swath SWH, which is retrieved by combining the observations of  
190 both SWIM and SCAT from the DNN model, provides not only a significantly improved spatial  
191 coverage but also an accuracy comparable to that of altimeter observations.

192

#### 193 **4 Impact of Wide Swath SWH on Data Assimilation**

194 With the increased spatial coverage and good accuracy, wide swath SWH data have the  
195 potential to enhance the assimilation of data in wave models compared with the assimilation of  
196 nadir data only. Therefore, a set of assimilation experiments is performed to investigate this topic.  
197 The assimilation experiments are implemented using the wave model MFWAM, which is a 3rd-  
198 generation numerical wave forecast model that is applied during the operational forecasts of  
199 Meteo France. The assimilation system of the MFWAM model can jointly use altimeter SWH  
200 and directional wave spectra parameters from SAR or CFOSAT observations (Lefèvre et al.,  
201 2012). The MFWAM model has demonstrated good accuracy in a validation against buoy data  
202 (Bidlot, 2017).

203 As indicated in Table 1, four model runs are performed, including three runs with the  
204 assimilation of wide swath SWH and nadir SWH (Run A), wide swath SWH only (Run B), and  
205 SWH from nadir only (Run C); in addition, a control run without any assimilation is also  
206 conducted. The SWH observations are assimilated into MFWAM by using optimal interpolation  
207 (Aouf et al., 2015) with a 3-hour time window ( $\pm 1.5$  hours). The model runs globally with a  
208 spatial resolution of  $0.5^\circ$  and is forced by 3-hourly wind and sea ice fraction fields provided by  
209 the IFS-ECMWF atmospheric system. The time period of the model experiments is May 2019.  
210 The SWH observations from National Data Buoy Center (NDBC) buoys are used as the  
211 reference to assess the accuracy of each run. A total of 45 NDBC buoys with distances off the  
212 coast beyond 60 km are selected for the assessment. From the 7377 matchups with buoys, the  
213 results of the validations are presented in Table 1. First, all three runs with assimilation achieved  
214 improved error statistics compared to the control run, reflecting the positive impacts of

215 assimilation. From the comparison between Run B and Run C, which employ an approximately  
 216 equal number of SWH observations, the assimilation of the wide swath SWH resulted in a lower  
 217 RMSE, NRMSE and SI than the assimilation of the nadir SWH only and is degraded only in the  
 218 bias. Therefore, we can say that, with the increased number of observations and the acceptable  
 219 accuracy, the newly retrieved wide swath SWH obtains an almost equivalent assimilation effect  
 220 as nadir observations. Therefore, it is reasonable that Run A, which assimilates both wide swath  
 221 and nadir SWH, achieves better values of the RMSE (which improved from 0.319 m for Run C  
 222 to 0.302 m for Run A), NRMSE (from 18.88% for Run C to 17.85%) and SI (from 18.74 for Run  
 223 C to 17.65) than the assimilation of nadir SWH only, although the bias is nonsignificantly  
 224 degraded from -0.038 to -0.044. Consequently, the addition of wide swath SWH enhances the  
 225 positive impact of the assimilation of traditional nadir observations.

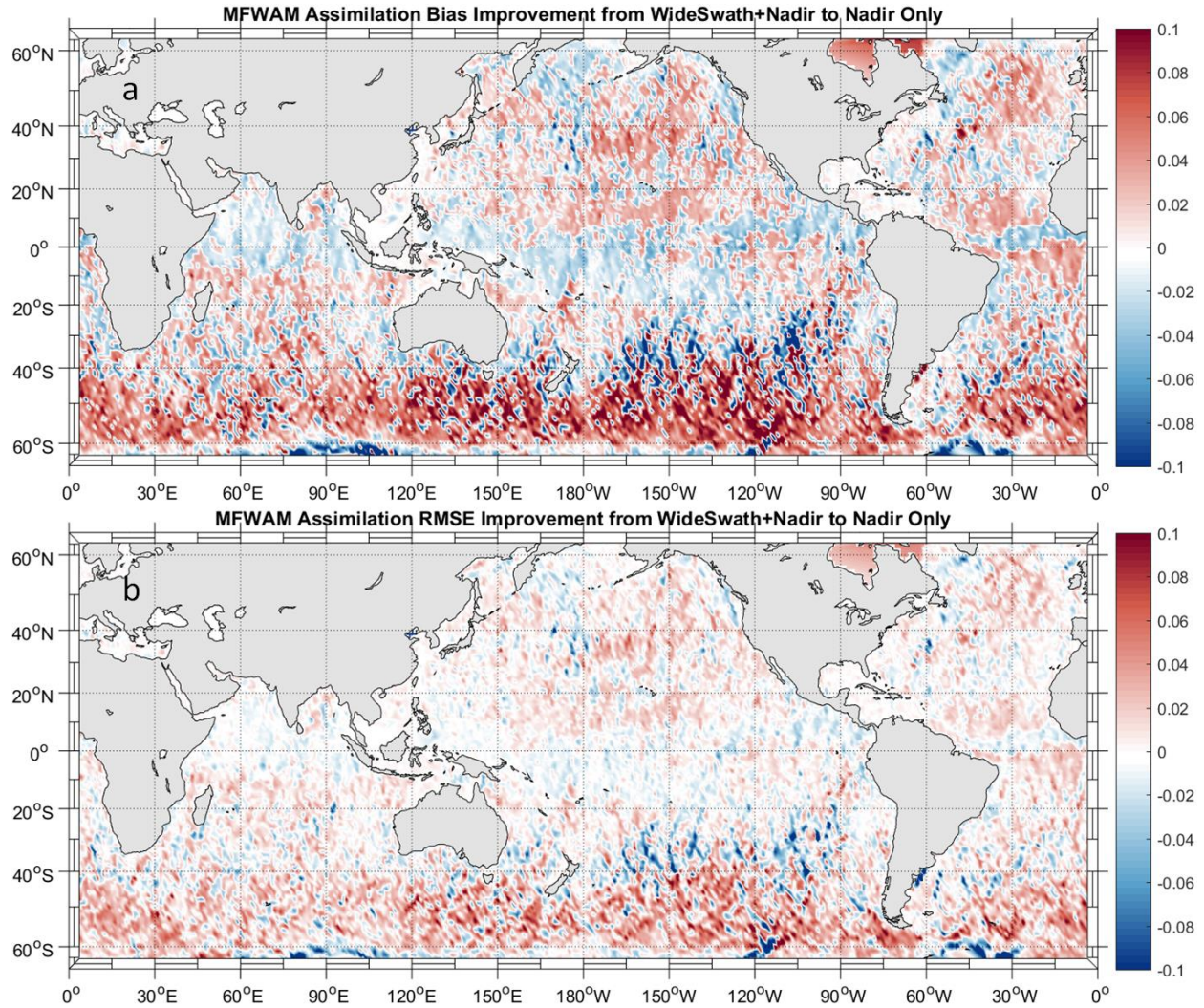
226 Table 1. *Setups of the assimilation runs and their validations against NDBC buoys*

Runs	Assimilated Data	Bias (m)	RMSE (m)	NRMSE (%)	SI (%)
A	Wide Swath SWH, Nadir SWH	-0.044	0.302	17.85	17.65
B	Wide Swath SWH only	-0.066	0.306	18.09	17.66
C	Nadir SWH only	-0.038	0.319	18.88	18.74
CTRL	No	-0.111	0.343	20.32	19.22

227 As the NDBC buoys are located mainly in the Northeast Pacific and West Atlantic, the  
 228 assimilation impact on the global wave system is further investigated by using the Jason-3 and  
 229 SARAL altimeters. As the significant positive impact of assimilation is clearly seen in Table 1,  
 230 here, we focus more on the improvements between Run A and Run C. To illustrate the positive  
 231 assimilation effect of the addition of the wide swath SWH in a more obvious way, the  
 232 improvements in the bias and RMSE are defined as follows:

$$233 \quad bias_{imp} = |bias_{Rc}| - |bias_{Ra}| \quad (1) \quad RMSE_{imp} = RMSE_{Rc} - RMSE_{Ra} \quad (2)$$

234 where the subscript ‘imp’ indicates an improvement and the subscripts ‘Rc’ and ‘Ra’ indicate the  
 235 parameters from Run A and Run C, respectively. Therefore, it can be inferred that when Run A  
 236 gives a lower bias or RMSE, the improvement parameter would be positive; in contrast,  
 237 degradation would lead to a negative value.



238

239 **Figure 3.** Distribution of the improvements in Run A relative to Run C. The improvements of  
 240 the bias and RMSE are indicated in panels 3a and 3b, respectively.

241 The global distributions of the improvements due to the addition of the wide swath SWH  
 242 are presented in Figure 3. Red color represents a positive improvement, that is, a lower bias or  
 243 RMSE, while blue reflects degraded accuracy. With the assimilation of both wide swath SWH  
 244 and nadir SWH, improvements can be found in most of the global ocean, as red is dominant in  
 245 both Figure 3a and Figure 3b, especially in the mid-latitude regions. As indicated in Figure 3a,  
 246 the most significant improvement in the bias occurred in the mid-latitude oceans of the Southern  
 247 Hemisphere between 40°S and 60°S, where the bias was reduced by an average of 0.1 m.  
 248 Obvious bias improvements are also observed in the North Pacific and most of the Atlantic.  
 249 Slight degradations in the bias appear mainly in the tropical oceans, where the SWH is lower

250 than in the subtropical and mid-latitude oceans. The distribution of the RMSE improvement is  
251 similar to that of the bias improvement, showing general improvement globally. Specifically,  
252 positive impacts on the bias and RMSE are achieved for 65.0% and 62.5% of the global ocean,  
253 respectively, when the wide swath SWH is assimilated with the nadir SWH. We note that the  
254 slight degradation can be explained by the lack of scaling in the model and the observation errors  
255 used in the optimal interpolation of the assimilation scheme. Optimization of the assimilation  
256 scheme for the wide swath SWH should be considered before the implementation of operational  
257 applications.

258

## 259 **5 Conclusions and Discussion**

260 The accuracy of wave simulations from numerical wave models can be effectively  
261 improved by assimilating all available observations, including the remotely sensed SWH from  
262 spaceborne altimeters. And the impact of wave assimilation is highly related to the quantity of  
263 the observations.

264 CFOSAT is a new and unique oceanographic satellite equipped with two sensors, namely,  
265 SWIM and SCAT, which provide simultaneous observations of waves and surface winds.  
266 Although SWIM provides information in two additional columns of ‘boxes’ on either side of the  
267 nadir track, the spatial coverage of SWIM data remains limited. SCAT observations, in contrast,  
268 provide wind observations over a large swath (approximately 800 km). Since the wind speeds  
269 observed by SCAT are highly related to the wave state, a method for obtaining the SWH over a  
270 wider swath (with respect to only the nadir track) is presented that makes use of wind speed  
271 measurements from SCAT and wave observations from SWIM simultaneously. A retrieval  
272 method for obtaining the wide swath SWH is constructed based on a deep neural network. The  
273 major inputs of the DNN model are the SWH and sigma0 from the SWIM nadir observations, the  
274 SWH and peak period from the wave spectra in the SWIM off-nadir boxes, and the wind speed  
275 from SCAT. The training of the deep neural network is carried out by using collocated  
276 independent SWH altimeter observations. The model is then used to estimate the SWH at SCAT  
277 grid points to provide the SWH over an extended spatial coverage.

278 In addition to the significantly increased number of observations, the wide swath SWH has  
279 been shown to achieve good accuracy based on independent validations against altimeters.  
280 Therefore, a set of assimilation runs is implemented to assess the potential impact of the wide  
281 swath SWH. Promising results are found from a validation against NDBC buoy wave  
282 observations. The assimilation of the wide swath SWH achieves an equivalent positive impact to  
283 the assimilation of SWIM nadir SWH observations. It should be noted that the assimilation of the  
284 wide swath SWH achieves lower values of the RMSE, NRMSE and scatter index. Assessing the  
285 SWH from altimeters, a global validation also presents a satisfactory conclusion that, together  
286 with traditional nadir SWH observations, the addition of the wide swath SWH does enhance the  
287 positive impact of the assimilation. The enhancements produced by assimilating the wide swath  
288 SWH occur mainly in the subtropical and mid-latitude oceans where non-fully-developed wind  
289 seas are dominant.

290 The success of the wide swath SWH estimation comes from the setup of CFOSAT payloads,  
291 which provide synchronous observations of waves and winds from SWIM and SCAT,  
292 respectively. To a certain extent, the wide swath SWH combines the advantages of both SWIM  
293 and SCAT, thereby obtaining significantly increased spatial coverage and reasonable accuracy.  
294 As evidenced by the assimilation experiments, the wide swath SWH also has an enhanced  
295 positive impact on the wave model accuracy. Therefore, this research provides insights into how  
296 we can increase the usage efficiency of ocean remote sensing.

297 It is also worth noting that CFOSAT is not the only satellite carrying both wind and wave  
298 instruments. The HY2 series, including the HY2A (Wang et al., 2013), the HY2B (Jia et al.,  
299 2020) and the most recently launched HY2C satellites, are all equipped with both an altimeter  
300 and a scatterometer, giving them the ability to monitor nadir waves and wide swath winds  
301 simultaneously. However, further research is needed on the synchronous remote sensing based  
302 observation of winds and waves. Although the acquisition of the wide swath SWH provides  
303 evidence for the potential of these synchronous observations, the wide swath SWH estimation  
304 must be further perfected. For instance, in this paper, the swath of the SWH is limited to 200 km,  
305 while a naturally wider swath would achieve more observations; however, a swath that is too  
306 wide would also degrade the accuracy because greater distance from the nadir track may lead to  
307 larger deviations for the assimilation. Therefore, more work should be conducted to optimize the  
308 SWH swath to obtain the maximum positive impact on wave assimilation. Furthermore, because

309 the wind and wave states are highly coupled, the synchronous observation of winds and waves  
310 from satellites such as CFOSAT and the HY2 series would provide valuable information on  
311 wind-wave interactions and related topics.

312

### 313 **Acknowledgments and Data**

314 The authors would like to thank the Centre National d'Études Spatiales (CNES) for  
315 providing the CFOSAT SWIM and SCAT data (accessible at ftp-access.aviso.altimetry.fr for the  
316 science team members of CFOSAT). We thank the Aviso User Service for the data from the  
317 Jason-3 and SARAL altimeters (accessible at aviso-data-center.cnes.fr). We would also like to  
318 thank the National Data Buoy Center (NDBC) for providing the buoy data with high quality  
319 (accessible at ndbc.noaa.gov).

320 This research was funded by the National Key Research and Development Program of  
321 China (Grant No. 2016YFC1401701 and 2016YFC1402703) and the Laboratory for Regional  
322 Oceanography and Numerical Modeling, Pilot National Laboratory for Marine Science and  
323 Technology (Grant No. 2019B03).

324 The authors would also like to thank Malek Ghantous for reading the manuscript and  
325 correcting the language.

326

### 327 **References**

- 328 Abdalla, S. (2015). SARAL/AltiKa wind and wave products: monitoring, validation and  
329 assimilation. *Marine Geodesy*, 38(sup1), 365–380.
- 330 Aouf, L., & Lefèvre, J.-M. (2015). On the impact of the assimilation of SARAL/AltiKa wave  
331 data in the operational wave model MFWAM. *Marine Geodesy*, 38(sup1), 381–395.
- 332 Bhatt, V., Kumar, R., Basu, S., & Agarwal, V. K. (2005). Assimilation of altimeter significant  
333 wave height into a third-generation global spectral wave model. *IEEE Transactions on*  
334 *Geoscience and Remote Sensing*, 43(1), 110–117.
- 335 Bidlot, J. R. (2017). Twenty-one years of wave forecast verification. *ECMWF Newsletter*, 150,  
336 31–36.

- 337 Breivik, L.-A., & Reistad, M. (1994). Assimilation of ERS-1 altimeter wave heights in an  
 338 operational numerical wave model. *Weather and Forecasting*, 9(3), 440–451.
- 339 Cao, L., Hou, Y., & Qi, P. (2015). Altimeter significant wave height data assimilation in the  
 340 South China Sea using Ensemble Optimal Interpolation. *Chinese Journal of Oceanology  
 341 and Limnology*, 33(5), 1309–1319.
- 342 Cotton, P. D., & Carter, D. J. T. (1994). Cross calibration of TOPEX, ERS-I, and Geosat wave  
 343 heights. *Journal of Geophysical Research: Oceans*, 99(C12), 25025–25033.
- 344 Daley, R. (1993). *Atmospheric data analysis*. Cambridge university press.
- 345 Dobson, E., Monaldo, F., Goldhirsh, J., & Wilkerson, J. (1987). Validation of Geosat  
 346 altimeter-derived wind speeds and significant wave heights using buoy data. *Journal of  
 347 Geophysical Research: Oceans*, 92(C10), 10719–10731.
- 348 Emmanouil, G., Galanis, G., Kallos, G., Breivik, L. A., Heiberg, H., & Reistad, M. (2007).  
 349 Assimilation of radar altimeter data in numerical wave models: an impact study in two  
 350 different wave climate regions. In *Annales Geophysicae* (Vol. 25, pp. 581–595). Copernicus  
 351 GmbH.
- 352 Fedor, L. S., Godbey, T. W., Gower, J. F. R., Guptill, R., Hayne, G. S., Rufenach, C. L., &  
 353 Walsh, E. J. (1979). Satellite altimeter measurements of sea state—An algorithm  
 354 comparison. *Journal of Geophysical Research: Solid Earth*, 84(B8), 3991–4001.
- 355 Hasselmann, D. E., Dunckel, M., & Ewing, J. A. (1980). Directional wave spectra observed  
 356 during JONSWAP 1973. *Journal of Physical Oceanography*, 10(8), 1264–1280.
- 357 Hauser, D., Tison, C., Amiot, T., Delaye, L., Mouche, A., Guitton, G., et al. (2016). CFOSAT: A  
 358 new Chinese-French satellite for joint observations of ocean wind vector and directional  
 359 spectra of ocean waves. In *Remote Sensing Of The Oceans And Inland Waters: Techniques,  
 360 Applications, And Challenges* (Vol. 9878, p. 98780T). International Society for Optics and  
 361 Photonics.
- 362 Hauser, D., Tourain, C., Hermozo, L., Alraddawi, D., Aouf, L., Chapron, B., et al. (2020). New  
 363 Observations From the SWIM Radar On-Board CFOSAT: Instrument Validation and Ocean  
 364 Wave Measurement Assessment. *IEEE Transactions on Geoscience and Remote Sensing*.
- 365 Hayne, G. (1980). Radar altimeter mean return waveforms from near-normal-incidence ocean  
 366 surface scattering. *IEEE Transactions on Antennas and Propagation*, 28(5), 687–692.
- 367 Jia, Y., Yang, J., Lin, M., Zhang, Y., Ma, C., & Fan, C. (2020). Global Assessments of the HY-  
 368 2B Measurements and Cross-Calibrations with Jason-3. *Remote Sensing*, 12(15), 2470.
- 369 Jiang, X., Lin, M., Liu, J., Zhang, Y., Xie, X., Peng, H., & Zhou, W. (2012). The HY-2 satellite  
 370 and its preliminary assessment. *International Journal of Digital Earth*, 5(3), 266–281.

- 371 Lefèvre, J.-M., & Aouf, L. (2012). Latest developments in wave data assimilation. In *ECMWF*  
 372 *Workshop on Ocean Waves* (pp. 25–27).
- 373 Lin, W., Dong, X., Portabella, M., Lang, S., He, Y., Yun, R., et al. (2018). A perspective on the  
 374 performance of the CFOSAT rotating fan-beam scatterometer. *IEEE Transactions on*  
 375 *Geoscience and Remote Sensing*, 57(2), 627–639.
- 376 Lionello, P., Günther, H., & Janssen, P. A. E. M. (1992). Assimilation of altimeter data in a  
 377 global third-generation wave model. *Journal of Geophysical Research: Oceans*, 97(C9),  
 378 14453–14474.
- 379 Liu, Q., Babanin, A. V, Guan, C., Zieger, S., Sun, J., & Jia, Y. (2016). Calibration and validation  
 380 of HY-2 altimeter wave height. *Journal of Atmospheric and Oceanic Technology*, 33(5),  
 381 919–936.
- 382 Nair, V., & Hinton, G. E. (2010). Rectified linear units improve restricted boltzmann machines.  
 383 In *ICML*.
- 384 Nerem, R. S., Chambers, D. P., Choe, C., & Mitchum, G. T. (2010). Estimating mean sea level  
 385 change from the TOPEX and Jason altimeter missions. *Marine Geodesy*, 33(S1), 435–446.
- 386 Portilla, J. (2009). Buoy Data Assimilation in Nearshore Wave Modelling (Assimilatie van  
 387 boeigegevens in de modellering van golven nabij de kust).
- 388 Steele, K. E., Teng, C.-C., & Wang, D. W. C. (1992). Wave direction measurements using pitch-  
 389 roll buoys. *Ocean Engineering*, 19(4), 349–375.
- 390 Wang, J., Zhang, J., & Yang, J. (2013). The validation of HY-2 altimeter measurements of a  
 391 significant wave height based on buoy data. *Acta Oceanologica Sinica*, 32(11), 87–90.
- 392 Wang, J., Aouf, L., Jia, Y., & Zhang, Y. (2020). Validation and Calibration of Significant Wave  
 393 Height and Wind Speed Retrievals from HY2B Altimeter Based on Deep Learning. *Remote*  
 394 *Sensing*, 12(17), 2858.
- 395 Xu, Y., Liu, J., Xie, L., Sun, C., Liu, J., Li, J., & Xian, D. (2019). China-France Oceanography  
 396 Satellite (CFOSAT) simultaneously observes the typhoon-induced wind and wave fields.  
 397 *Acta Oceanologica Sinica*, 38(11), 158–161.
- 398 Yang, J., Zhang, J., Jia, Y., Fan, C., & Cui, W. (2020). Validation of Sentinel-3A/3B and Jason-3  
 399 Altimeter Wind Speeds and Significant Wave Heights Using Buoy and ASCAT Data.  
 400 *Remote Sensing*, 12(13), 2079.